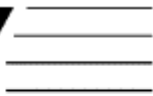


CHEMISTRY 
A EUROPEAN JOURNAL

Supporting Information

© Copyright Wiley-VCH Verlag GmbH & Co. KGaA, 69451 Weinheim, 2005

**A Multisite Molecular Mechanism for Baeyer-Villiger Oxidations on
Solid Catalysts Using Environmentally Friendly H₂O₂ as Oxidant**

Mercedes Boronat, Avelino Corma, Michael Renz, Germán Sastre, Pedro M. Viruela

Supporting information concerning the parameterisation of a forcefield for Sn/Si zeolites.

An empirical fitting technique has been used to find the parameters of the new forcefield and this consists of minimizing the difference between observed and calculated properties by means of a least squares procedure. Concurrent fitting of multiple structures is found to enhance greatly the reliability of the derived potentials and generally leads to more physically reasonable potentials without the use of constraints. In our case, we are interested in Si/Sn-based zeolites and therefore we have included in the fit the structures of quartz^[1] and SnO₂.^[2] Apart from the structure, it is also vital to incorporate data regarding the curvature of the energy surface about the minima. The bulk module are included^[1,3] as well as the elastic constants and the highest phonon frequency of quartz.^[1]

The relaxed fitting scheme^[4] is employed for the final refinement of the potential parameters, as implemented within the program GULP.^[5] The potential model which has been used is the Born model with inclusion of dipolar polarization of oxygen, as it was done in most previous work,^[6] consists of the Coulomb interaction, evaluated via an Ewald summation, a short-range pair potential described by a Buckingham function with cut-off distance of 12 Å, and

three-body angle bending terms (O-Si-O and O-Sn-O). The shell model was used to simulate the polarisability of the oxygen ions. In the case of tin, the three-body bending term was used to reproduce the tendency to show octahedral coordination by an equilibrium angle of 90° , whereas for silicon the tetrahedral tendency is shown by an equilibrium angle in the three body term of 109.47° (see Table S1). A crucial concept to be bare in mind here is the fact that the octahedral tendency is the preferred Sn coordination (as indicated by the equilibrium angle O-Sn-O = 90° in Table S1), but does not preclude the fact that Sn may coordinate tetrahedrally, if the energetic penalty to open the O-Sn-O angles above 90° is paid at the expense of achieving a less stable configuration. Indeed, the energetic constraint for the Sn to coordinate tetrahedrally (as observed in Sn-zeolites), is not a drawback of the methodology but rather a feature, that reflects the experimental difficulty for Sn to have tetrahedral coordination.

The functional forms are as follows:

$$E^{quartz} = E^{Buckingham} + E^{threebody} + E^{core-shell} + E^{Coulombic} \quad (1)$$

$$E^{SnO_2} = E^{Buckingham} + E^{core-shell} + E^{Coulombic} \quad (2)$$

$$E_{ij}^{Buckingham} = A_{ij} \exp\left(-\frac{r_{ij}}{\rho_{ij}}\right) - \frac{C_{ij}}{r_{ij}^6} \quad (3)$$

$$E_{ijk}^{threebody} = \frac{1}{2} k_{ijk} (\theta - \theta_0)^2 \quad (4)$$

$$E_{ij}^{core-shell} = \frac{1}{2} k_{ij}^{cs} r_{ij}^2 \quad (5)$$

$$E_{ij}^{Coulombic} = \frac{q_i q_j}{4\pi\epsilon_0 r_{ij}} \quad (6)$$

There have been several previous attempts to extend the forcefield of Sanders *et al.* for silicates^[6] to other microporous framework materials, such as germania, trying to preserve the already defined aluminosilicate forcefield as unchanged, and to fit only the potential parameters that are left unconstrained by this requirement. However, when doing this, different conflicts appear that can be related to differences in the ionic character of the two materials. The same problem appears when trying a concurrent fitting for quartz and SnO₂. Thus, since both are treated as fully ionic solids in order to make defect problems facile to study, this must be compensated through the shell model parameters. Hence, the polarisability of oxygen within the shell model must be different for quartz and SnO₂. A

similar strategy to that used for Si/Ge zeolites reported in a previous study^[1] has been employed here and more details can be found there. The use of different oxygen parameters for the charges and the core-shell spring constants is established as shown in Table S1, whereas the short-range O-O potential is constrained to remain the same within the two phases.

The quality of a fit can be measured by the sum of the squares of the differences between the experimental and calculated values for the observables, multiplied by appropriate weighting factors. Here the weights used are 1000.0 for all unit cell parameters, 10000.0 for all fractional coordinates, and 1.0 for all properties. This reflects the fact that it is pointless to reproduce the curvature related properties, unless the structure is firstly reproduced. A final sum of squares of 0.12 is obtained within the above model, which is indicative of an excellent fit, and this can be confirmed by the comparison of experimental and calculated structural and physical properties of SnO₂ as shown in Table S2.

TABLE S1. Interatomic potential parameters for zeolites with Si,Sn as tetrahedral atoms. It is noted that this forcefield has been made compatible with the Si/Ge forcefield in a previous study,^[1] and therefore, both sets of forcefields can be merged in order to simulate Si/Ge/Sn zeolites.

Atomic charges

Atom	Core	Shell
Si	4.0	-
Sn	4.0	-
O in Sn-O-Sn	2.787415	-4.787415
O in Si-O-Si	0.870733	-2.870733
O in Sn-O-Si	1.947179	-3.947179

Buckingham

i	j	A_{ij} (eV)	ρ^{ij} (Å)	C_{ij} (eVÅ ⁶)
O shell	O shell	22764.0	0.149000	10.937044
Si core	O shell	1315.2478	0.317759	10.141118
Sn core	O shell	1881.8178	0.326922	0.00

Three body

i	j	k	k_{ijk} (eV rad ⁻²)	θ_0 (deg)
O shell	Si core	O shell	1.2614	109.47
O shell	Sn core	O shell	0.8004	90.00

Spring

i	j	k_{ij}^{es} (eVÅ ⁻²)
O(Sn-O-Sn) core	O(Sn-O-Sn) shell	291.84690
O(Si-O-Si) core	O(Si-O-Si) shell	75.96980
O(Sn-O-Si) core	O(Sn-O-Si) shell	183.90835

TABLE S2. Experimental and calculated values of structural and physical parameters of SnO₂. The parameterization has been carried within the cubic group P4₂/mmm (#136). The SnO₂ has a rutile type structure with a distorted hexagonal close packing for the oxygen anions (whose coordination is 3) and with the tin cations occupying half of the octahedral sites. The calculations have been performed with our parameterized forcefield indicated in Table S1 and the units are volume in Å³, crystallographic parameters in Å, and bulk modulus in GPa.

Parameter	Experimental	Calculated
Volume	71.50787	71.519243
a	4.73727	4.738060
b	4.73727	4.738060
c	3.18638	3.185824
1 x	0.00000	0.00000
1 y	0.00000	0.00000
1 z	0.00000	0.00000
2 x	0.30700	0.310507
2 y	0.30700	0.310507
2 z	0.00000	0.00000
3 x	0.30700	0.313679
3 y	0.30700	0.313679
3 z	0.00000	0.00000
Bulk Modulus	218.00000	218.24458

References

- [1] G. Sastre, J. D. Gale, *Chem. Mater.* **2003**, *15*, 1788-1796.
- [2] W. H. Baur, *Acta Crystallogr.* **1971**, *56*, 1573-1599.
- [3] S. J. Chakravorty, E. Clementi, *Phys. Rev. A* **1989**, *39*, 2290-2296.
- [4] J. D. Gale, *Philos. Magaz. B* **1996**, *73*, 3-19.
- [5] J. D. Gale, *J. Chem. Soc. Faraday Trans.* **1997**, *93*, 629-637.
- [6] a) M. J. Sanders, M. Leslie, C. R. A. Catlow, *J. Chem. Soc. Chem. Commun.* **1984**, 1271-1273; b) R. A. Jackson, C. R. A. Catlow, *Mol. Simul.* **1988**, *1*, 207-224.

Supporting information concerning the kinetics of the Baeyer-Villiger oxidation of cyclohexanone by hydrogen peroxide catalyzed by Sn-Beta

In order to reduce the number of parameters in equation (1)

$$r_0 = \frac{k[CH]_0[HP]_0}{(1 + K_a[CH]_0 + K_b[HP]_0 + K_c[WA]_0)(1 + K_d[HP]_0 + K_e[WA]_0)} \quad (1)$$

the following approximations have been considered: we have assumed that the adsorption constant for H₂O₂ is the same at the two sites ($K_b = K_d$), and the same applies for the adsorption of water ($K_c = K_e$). By doing this, equation (1) transforms into (6):

$$r_0 = \frac{k[CH]_0[HP]_0}{(1 + K_a[CH]_0 + K_b[HP]_0 + K_c[WA]_0)(1 + K_b[HP]_0 + K_c[WA]_0)} \quad (6)$$

Then, initial reaction rates were calculated by dividing conversion by time, at levels of conversion below 10%, and working under the following experimental conditions: (A) working with an excess of cyclohexanone and changing the initial concentrations of hydrogen peroxide/water as limiting reactant; (B) studying the effect of water in the presence of the same excess of

cyclohexanone as in (A) with hydrogen peroxide as limiting substrate; and (C) changing the initial concentration of cyclohexanone in presence of an excess of hydrogen peroxide/water. By working under reaction conditions A, B and C, equation (6) was reduced to (7), (8), (9) and (10)

$$m = \frac{1}{a} = \frac{1 + K_a[CH]_A}{k[CH]_A} \quad (7)$$

$$p = \frac{K_c}{b} = \frac{K_c(1 + K_a[CH]_B)}{k[CH]_B[HP]_B} \quad (8)$$

$$q = \frac{c}{b} = \frac{(1 + K_b[HP]_B)(1 + K_a[CH]_B)}{k[CH]_B[HP]_B} \quad (9)$$

$$s = d = \frac{k}{(K_b + 3.5K_c)^2[HP]_C} \quad (10)$$

which, after linearization become (2), (3), (4) and (5), respectively

$$K_c = \frac{p[HP]_B}{m} \quad (2)$$

$$K_b = \frac{q[HP]_B - 1}{\frac{m}{[HP]_B}} \quad (3)$$

$$k = s(K_b + 3.5K_c)^2[HP]_C \quad (4)$$

$$K_a = \frac{mk[CH]_A - 1}{[CH]_A} \quad (5)$$

The three different conditions A, B and C were employed at three different temperatures, namely 60, 70, and 80 °C. For each of these nine reaction sets at least four

concentrations of the variable component have been chosen. The complete sets of all these concentrations are given in Table S3. The resulting initial rates are summarized in the Tables S4 to S6. The initial rates are converted into the corresponding graphics depicted in Figures 8 to 10 (cf. journal article). From these graphics m, p, q, and s can be distilled for each temperature and the constants k and K_a to K_c calculated. These data are represented in Table 5 (cf. journal article).

TABLE S3. Reactant concentrations in conditions A to C for the Baeyer-Villiger oxidation of cyclohexanone by hydrogen peroxide catalyzed by Sn-Beta (var = variable).

conditions	temp./°C	reaction number	CH	HP	WA
A	60	1	0.759	0.077	0.27
A	60	2	0.764	0.078	0.275
A	60	3	0.755	0.116	0.409
A	60	4	0.754	0.156	0.546
A	60	5	0.751	0.207	0.726
A	60	6	0.754	0.207	0.724
∅ 60A			0.756	var	var
B	60	1	0.772	0.093	0.175
B	60	2	0.770	0.094	0.351
B	60	3	0.759	0.095	0.521

S-13

B	60	4	0.760	0.097	0.699
∅ 60B			0.765	0.0948	var
C	60	1	0.028	0.791	2.774
C	60	2	0.044	0.791	2.774
C	60	3	0.056	0.783	2.745
C	60	4	0.074	0.776	2.722
∅ 60C			var	0.785	2.754
A	70	1	0.763	0.079	0.277
A	70	2	0.761	0.118	0.412
A	70	3	0.763	0.149	0.524
A	70	4	0.753	0.156	0.547
A	70	5	0.758	0.199	0.698
A	70	6	0.763	0.207	0.726
∅ 70A			0.760	var	var
B	70	1	0.762	0.088	0.167
B	70	2	0.756	0.088	0.328
B	70	3	0.755	0.088	0.493
B	70	4	0.751	0.088	0.655
∅ 70B			0.756	0.088	var
C	70	1	0.026	0.777	2.729
C	70	2	0.040	0.774	2.724
C	70	3	0.053	0.774	2.725
C	70	4	0.071	0.773	2.724
∅ 70C			var	0.775	2.726
A	80	1	0.740	0.078	0.273
A	80	2	0.761	0.117	0.411
A	80	3	0.756	0.155	0.543

S-14

A	80	4	0.763	0.156	0.546
A	80	5	0.753	0.205	0.720
A	80	6	0.756	0.208	0.728
∅ 80A			0.754	var	var
B	80	1	0.762	0.088	0.167
B	80	2	0.756	0.088	0.328
B	80	3	0.755	0.088	0.493
B	80	4	0.751	0.088	0.655
∅ 80B			0.756	0.088	var
C	80	1	0.027	0.777	2.727
C	80	2	0.040	0.774	2.715
C	80	3	0.053	0.78	2.735
C	80	4	0.071	0.775	2.717
∅ 80C			var	0.777	2.724

TABLE S4. Different concentrations of hydrogen peroxide in conditions A at three different temperatures and the resulting initial rates.

entry	temp.	[HP]	1/[HP]	initial rate	1/rate
1	60	0.077	13.0	0.0319	31.4
2	60	0.078	12.8	0.0310	32.3
3	60	0.116	8.62	0.0355	28.2
4	60	0.156	6.41	0.0408	24.5
5	60	0.207	4.83	0.0467	21.4
6	60	0.207	4.83	0.0425	23.5
7	70	0.079	12.7	0.0616	16.2
8	70	0.118	8.47	0.0760	13.2
9	70	0.149	6.71	0.0754	13.3
10	70	0.156	6.41	0.0781	12.8
11	70	0.199	5.03	0.0804	12.4
12	70	0.207	4.83	0.0870	11.5
13	80	0.078	12.8	0.129	7.75
14	80	0.117	8.55	0.166	6.02
15	80	0.155	6.45	0.171	5.85
16	80	0.156	6.41	0.163	6.13
17	80	0.205	4.88	0.177	5.65
18	80	0.208	4.81	0.181	5.52

TABLE S5. Different concentrations of water in conditions B at three different temperatures and the resulting initial rates.

entry	temp./°C	[WA]	initial rate	1/rate
1	60	0.175	0.0454	22.0
2	60	0.351	0.0360	27.8
3	60	0.521	0.0298	33.6
4	60	0.699	0.0243	41.1
5	70	0.167	0.0955	10.5
6	70	0.328	0.0837	11.9
7	70	0.493	0.0651	15.4
8	70	0.655	0.0552	18.1
9	80	0.167	0.203	4.92
10	80	0.328	0.165	6.08
11	80	0.493	0.146	6.85
12	80	0.655	0.114	8.79

TABLE S6. Different concentrations of cyclohexanone in conditions C at three different temperatures and the resulting initial rates.

entry	temp.	[CH]	initial rate
1	60	0.028	0.00260
2	60	0.044	0.00455
3	60	0.056	0.00512
4	60	0.074	0.00595
5	70	0.026	0.00368
6	70	0.040	0.00616
7	70	0.053	0.00898
8	70	0.071	0.01198
9	80	0.027	0.00762
10	80	0.040	0.0121
11	80	0.053	0.0144
12	80	0.071	0.0219

Supporting information concerning the theoretical study of
mechanism 1 with model B-w

TABLE S7. Optimized values of the most important distances (Å) of the structures involved in mechanism 1 calculated with model B-w to simulate the catalyst active site. The atom labelling is shown in Figure 3.

	R1	TS1	CI1	TS2	P1
rSn-O _c	2.158	2.057	2.013	2.040	2.203
rO _c -C	1.243	1.287	1.379	1.323	1.235
rC-O _a	2.734	1.895	1.447	1.329	1.314
rO _a -O _b	1.439	1.431	1.463	1.841	3.276
rO _a -H _a	0.998	1.130	1.680 ^[a]	1.150 ^[a]	0.984 ^[a]
rO ₅ -H _a	1.647	1.282	0.993	1.252	1.749
rSn-O ₅	1.976	2.045	2.234	2.052	1.956
^[a] rO _b -H _a					